

**Investigation on temperature-dependent electrical
conductivity of carbon nanotube/epoxy composites for
sustainable energy applications**

**Michael K. Njuguna^a, Dilini Galpaya^a, Cheng Yan^{a*}, John M. Colwell^a, Geoffrey
Will^a, Ning Hu^b, Prasad Yarlagadda^a and John M. Bell^a**

*^a School of Chemistry, Physics and Mechanical Engineering , Queensland University
of Technology, GPO Box 2434, Brisbane QLD 4000, Australia.*

*^bDepartment of Mechanical Engineering, Chiba University, Yayoi-cho 1-33, Inage-
ku, Chiba 263-8522, Japan*

*Corresponding author, Fax: +61 7 3138 1516

Email address: c2.yan@qut.edu.au (Cheng Yan)

Abstract

Composites with carbon nanotubes are becoming increasingly used in energy storage and electronic devices, due to incorporated excellent properties from carbon nanotubes and polymers. Although their properties make them more attractive than conventional smart materials, their electrical properties are found to be temperature-dependent which is important to consider for the design of devices. To study the effects of temperature in electrically conductive multi-wall carbon nanotube/epoxy composites, thin films were prepared and the effect of temperature on the resistivity, thermal properties and Raman spectral characteristics of the composite films was evaluated. Resistivity-temperature profiles showed three distinct regions in as-cured samples and only two regions in samples whose thermal histories had been erased. In the vicinity of the glass transition temperature, the as-cured composites exhibited pronounced resistivity and enthalpic relaxation peaks, which both disappeared after erasing the composites' thermal histories by temperature cycling. Combined DSC, Raman spectroscopy, and resistivity-temperature analyses indicated that this phenomenon can be attributed to the physical aging of the epoxy matrix and that, in the region of the observed thermal history-dependent resistivity peaks, structural rearrangement of the conductive carbon nanotube network occurs through a volume expansion/relaxation process. These results have led to an overall greater understanding of the temperature-dependent behaviour of conductive carbon nanotube/epoxy composites, including the positive temperature coefficient effect.

Keywords: Carbon Nanotubes, Epoxy, Electrical Conductivity, Temperature Effect

1. INTRODUCTION

Carbon nanotubes (CNTs) demonstrate unusual properties and the presence of small amounts of nanotubes in an insulating polymeric matrix has been found to improve the mechanical properties as well as render the composite electrically conductive. CNTs exhibit high mechanical strength and electrical conductivity, while polymers provide good flexibility, high transparency, easy processing, and low cost. Therefore, polymer/CNT composites have received considerable attention and have been extensively investigated as a structural composite as well as a functional composite. In particular, due to the combined high conductivity, flexibility, stability, and transparency, polymer/CNT composites show great potential as electrode materials in a wide variety of fields such as organic solar cells, supercapacitors etc. Polymer/CNT composites are also identified as promising candidates for use as the active component of a variety of electronic devices such as field emitting displays, electrostatic magnetic interference shielding, intelligent coatings, and highly sensitive strain sensors¹⁻⁶. Huang et al. have recently fabricated novel dye-sensitized solar cells using aligned CNT/epoxy films as the counter electrodes as replacements of platinum or indium tin oxide in the solar cells. The practical application of platinum in dye-sensitized solar cells has been largely hindered by its high cost and less stability in many conditions such as dissolved in corrosive electrolytes, not resistance to acids. The CNT/polymer materials can efficiently resolve the above problems because they are cost-effective and stable⁷. It has also been reported that CNT/polymer nanocomposites are the most promising electrode materials for supercapacitors because of their excellent electrochemical charge storage properties and fast charge/discharge switching properties^{8, 9}. In addition to energy storage, the development of direction-sensitive bending strain sensors, consisting of a single block of CNT/epoxy composite, has been undertaken by generating a gradient in electrical conductivity throughout the material⁶.

A wealth of knowledge relating to percolation thresholds, conductivity changes with CNT orientation and dispersion, effects of surface treatment and other processing conditions of CNT/polymer composites is now available¹⁰⁻¹⁵. However, electrical characteristics of CNT/polymer composites are not stable and are influenced by environmental factors such as temperature which have yet to be well understood. Dramatic increases in the resistivity of conductive polymer composites have been observed at temperatures near the melting point or glass transition temperature of the polymer; a phenomenon known as the positive temperature coefficient (PTC) effect¹⁶⁻²⁰. Theories developed to explain the PTC effect include thermal expansion²¹, electron tunneling^{18, 22}, electric field emission²³ and residual stress release²⁴. These theories have not been well supported by experimental results and a consensus has not been reached on the dominant mechanism responsible for the PTC effect. In composites comprising crystalline or semi-crystalline polymers and conductive fillers, the PTC effect is caused by melting of the matrix crystallites^{17, 20}. The associated volume expansion and local matrix flow results in a large inter-filler distance, which in turn increases the tunneling resistance and thus increases the resistivity²². Volume expansion and matrix flow may also give rise to weak interactions between neighbouring fillers and reduce the number of conductive pathways, resulting in a significant increase in resistivity^{20, 25, 26}. The origins for the observed PTC effect in amorphous conductive polymer composites is less obvious and not well understood, with only limited research on this topic. It has been found that the increase of resistivity with temperature in amorphous thermoplastic polymer conductive composites is affected by the composite's thermal history²⁷ and for thermoset amorphous polymer conductive composites, even though the matrix phase volume expansion is very small near the T_g , significant changes in resistivity can occur in this temperature region¹⁶. Both of these studies identified the influence of the change in conducting filler network structure near T_g on the observed resistivity behaviour, but this behaviour was complex and

was effected by thermal history and polymer thermo-mechanical properties. Consequently, there is a need to investigate the exact origins of the so-called PTC effect in amorphous polymer conductive composites.

In the work presented here, the effects of temperature on the electrical resistivity of multi-wall carbon nanotube (MWCNT)/epoxy composites were evaluated. The changes that occur in the composite with changing temperature were assessed using Raman spectroscopy, thermal analysis and resistivity measurements. Our results suggest that the structural rearrangement of conductive fillers during an enthalpic relaxation event, which has its origins in the physical aging of the amorphous polymer, may contribute to this phenomenon.

2. EXPERIMENTAL

Materials

Chemical vapour deposition (CVD) synthesized multi-wall carbon nanotubes (Nano Carbon Technologies Corporation; Tokyo, Japan) with a purity of higher than 99.5% were used. The epoxy resin system was Araldite® GY191 cured with Aradur HY956. Both resin and hardener were supplied by CG Composites, Brisbane, Australia. Araldite® GY191 is predominantly diglycidyl ether of Bisphenol A (DGEBA), with Bisphenol-F epoxy resin and glycidyl ethers of C₁₂-C₁₄ alcohols as minor components. Aradur HY956 is a low viscosity polyamine hardener.

Sample preparation

The composites were prepared by dispersing up to 4% wt. of MWCNTs in the epoxy system with a planetary shear mixer (Thinky ARE-250, THINKY Corporation, Japan). First, Araldite® GY191 and Aradur HY956 were combined at a ratio of 4:1 and then shear-mixed for 30s. MWCNTs were then added and the mixture was shear-mixed for a further 60s at a mixing speed of 2000 rpm. A template with dimensions of 16 x 5mm, and a thickness of

120 μ m was used to cast the final mixture into thin films on a custom made circuit board with tin contacts for electrode connection. The samples were cured at room temperature for at least seven days, with post-curing at 100°C for 2 hours under argon.

Evaluation of electrical resistivity at different temperatures

Samples were placed in a VCL 4006 Votsch environment chamber and the temperature was varied between -20°C and 110°C at a heating and cooling rate of 2.5°C min⁻¹. An Agilent 34420A Micro-Ohm Meter was used to monitor the resistance. A K-type thermocouple connected to a National Instruments (NI) 9211 module/DAQ 9172 chassis was used to measure the temperature change.

Raman spectroscopy analysis

Raman spectra were collected using a Renishaw RamaScope connected to an Olympus BH-2 microscope with a 180° backscattering geometry. A CVI Melles Groit He-Ne laser (632.8 nm) was used for excitation through a $\times 50$ long working distance objective, which gave a spot size of approximately 1 μ m in diameter on the surface of the sample. A THMS 600 heating and cooling stage was used to vary the sample temperature from -160°C to 110°C. The instrument was calibrated prior to use using the 520.5cm⁻¹ line of a silicon wafer. Band intensities, widths and positions were obtained using Gaussian-Lorentzian routines fitted to the raw spectral data in Grams 32AI (6.00) spectral analysis software.

Thermal analysis

Differential scanning calorimetry (DSC) was conducted using a DSC Q100 (TA Instruments Inc.) under nitrogen atmosphere at a heating and cooling rate of 10°C min⁻¹ over the range, -20 to 120°C. To examine the effect of thermal history, two heat-cool-heat cycles with the above parameters were used.

Transmission electron microscopy (TEM) analysis

The morphology of MWCNTs was examined using a JEOL-2010 TEM. MWCNTs were dispersed in ethanol by shear mixing. A drop of the dispersed mixture was then cast on a carbon-coated copper grid and the ethanol allowed to evaporate in dry air. TEM images were acquired at an accelerating voltage of 200 kV.

Scanning electron microscopy (SEM) analysis

An FEI Quanta 200 Environmental SEM was used to examine epoxy/MWCNT composites. Small SEM samples were obtained by fracturing the cured epoxy/MWCNT composite samples across the thickness. The fractured samples were mounted on SEM stubs using carbon tape and then sputter-coated with a thin layer of gold to avoid charging during analysis. Parameters used for SEM analysis of the nanocomposite samples were: accelerating voltages of 15-25kV, a spot size of 2.5-4 mm and a working distance of between 9-10mm. Images were recorded at multiple sites to assess the dispersion, homogeneity and possible agglomeration of MWCNTs.

3. RESULTS AND DISCUSSION

Microstructure of MWCNTs and MWCNTs/epoxy composite

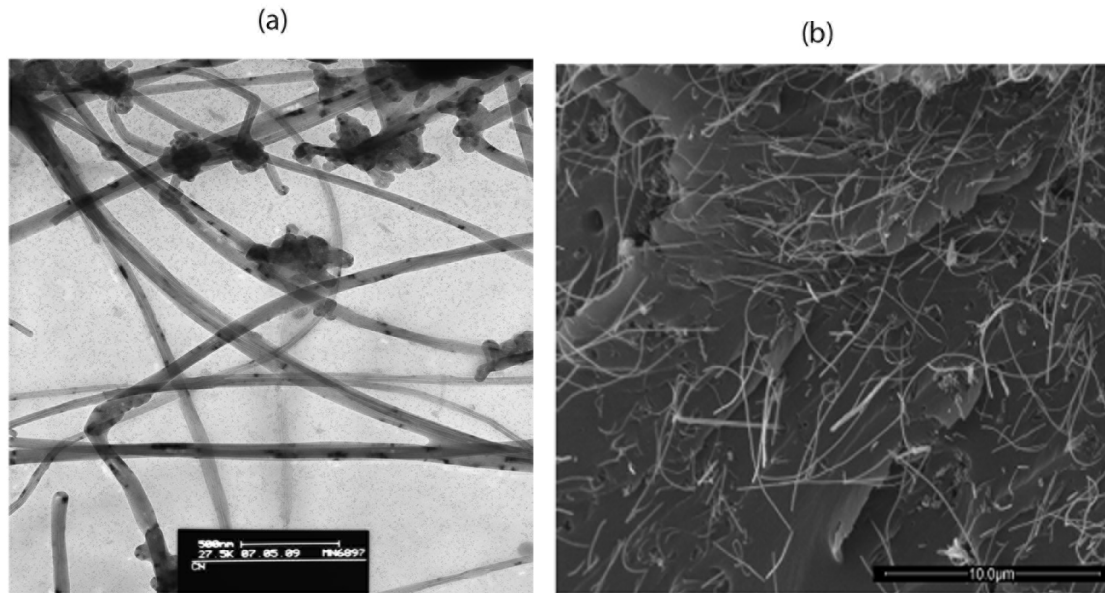


Fig. 1. (a) TEM image of MWCNTs (b) SEM image of the fractured surface of an epoxy composite with 3% wt. MWCNTs

The typical diameters and lengths of the pristine MWCNTs were in the range of 33-124 nm (average: 70 nm) and 1.1-22.5 μm (average: 8.7 μm) respectively, with a relatively straight morphology and little entanglement (Fig. 1a), which aided dispersal in the epoxy. SEM images of the fracture surfaces of epoxy composite samples were taken to assess the state of the MWCNT dispersion. Homogeneous and uniform dispersion of nanotubes is shown for a composite sample with a MWCNT loading of 3% wt. (Fig. 1b).

Effect of MWCNT loading on resistivity

Fig. 2 shows the dependence of room temperature resistivity of the composites on the MWCNT concentration. The resistivity changes from $\sim 10^{13} \Omega\text{m}$ (equivalent to unfilled epoxy resin²⁸) to a minimum of $\sim 10^1 \Omega\text{m}$ at 4% wt. MWCNTs, a decrease of 12 orders of magnitude. In general, the resistivity of a composite system above its percolation threshold can be described by the following scaling law²⁹,

$$\rho \propto (\psi - \psi_c)^{-t} \quad (1)$$

where ψ is the volume or weight fraction of the conducting filler, ψ_c is the percolation threshold and t is the critical exponent. The linear regression fit shown in the inset of Fig. 2 gave $t = 2.4 \pm 0.51$ and $\psi_c = 0.5 \pm 0.05$. Comparable values have been reported for other composite materials with CNT loadings in the range used in this study³⁰.

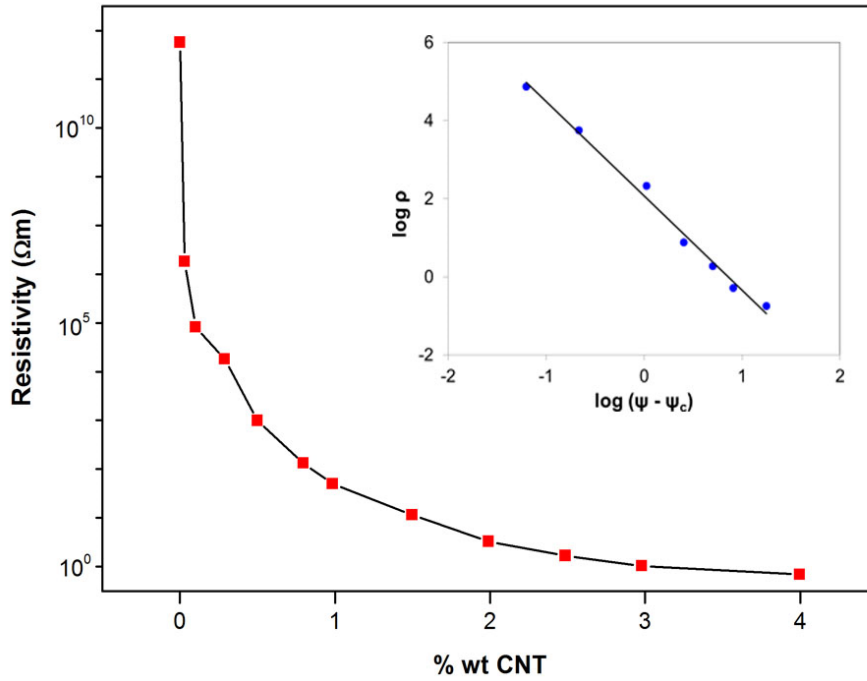


Fig. 2. Variation of resistivity with MWCNT loading (room temperature)

The effect of temperature on resistivity

The effect of temperature on resistivity of the MWCNT/epoxy composites was investigated using samples with 2 and 3% wt. MWCNT, from now on referred to as EP2 and EP3, respectively. These samples were selected because their CNT concentrations were well above the percolation threshold and they also had resistivity values close to saturation. Fig. 3 shows the effect of temperature on the resistivity of post-cured EP2 and EP3 samples. Three regions were observed in these plots. In the first region, the resistivity increased gradually in the low temperature range, followed by distinct resistivity peaks between 53 and 60°C and then a

period of recovery in which the percolating network rearranges, allowing for a reduction and then increase in the resistivity depending on the volume fraction of the epoxy matrix. In other studies on the temperature-resistivity characteristics of conductive polymer composites, it has been found that in the vicinity of the melting point or glass transition temperature of the polymer matrix, resistivity sharply increases with temperature^{16-20, 25-27, 31}; a phenomenon known as the positive temperature coefficient (PTC) effect.

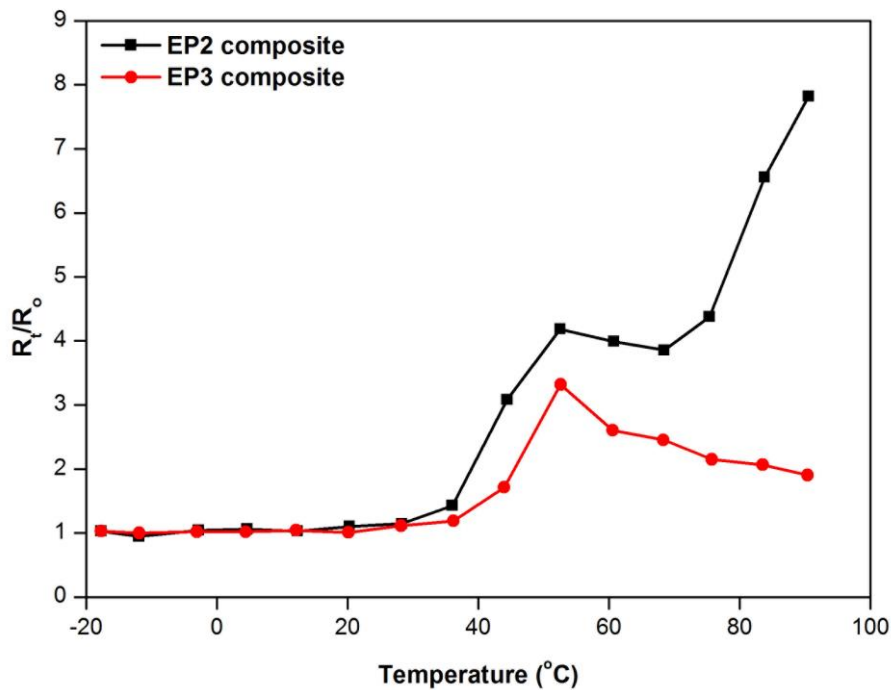


Fig. 3. Relative resistance versus temperature plots for post-cured EP2 and EP3 composite films. The R_t/R_0 ratio is used for ease of comparison, (R_0 for EP3 = 4036 Ω , R_0 for EP2 = 22067 Ω)

The PTC effect in conductive composites with crystalline or semi-crystalline polymer matrices occurs due to melting of the matrix crystallites²² and so many conductive crystalline and semi-crystalline polymeric composites exhibit a pronounced PTC effect. In contrast, only a few studies have reported the PTC effect in amorphous polymer composites^{16, 27, 31}. Klason and Kubat²⁷ found pronounced maxima in resistivity-temperature curves in amorphous thermoplastic polymers containing a small percentage of carbon black. The sharp resistivity

increase was observed only after the samples were stored for a certain period of time at temperatures lower than the glass transition temperature (T_g), or at heating rates substantially higher than those used in cooling the samples prior to the measurement. This suggests that physical aging of the polymer phase played a role in the PTC effects that were observed near T_g . Such effects can be studied using DSC.

DSC plots for samples EP2 and EP3 cured at room temperature for 7 days and subsequently post-cured at 100°C for 2 h under an argon atmosphere are shown in Fig. 4. When the samples were subjected to two DSC heat-cool-heat cycles, endothermic relaxation peaks were only observed during the first heating runs. Endothermic peaks were not observed during the subsequent three heating runs. In all cases, the endothermic peak temperature, as shown in Table 1 was lower than the T_g (calculated as the average of the midpoint temperature of the glass transition region for runs 2, 3 and 4).

Interestingly, the endothermic peaks (peak temperatures between 53 and 59°C) for the first DSC heating runs coincide with the resistivity peaks shown in Fig. 3. The sharp increase in resistivity was attributed to an increase in the inter-MWCNT distances caused by epoxy matrix expansion at temperatures close to T_g , resulting in higher tunneling resistance (illustrated in Fig. 9). However, following the peak in volume expansion, there is a period of recovery in which the percolating network re-arranges, allowing for a reduction and then increase in the resistivity depending on the volume fraction of the epoxy matrix. In addition, increased molecular mobility during the heating process may lead to a disruption of the nanotube network, causing a significant increase in resistivity. When a physically-aged amorphous polymer is heated above its T_g , the original thermodynamic state is recovered and the effects of aging are erased³². If the material is then cooled back to a temperature well below T_g and then immediately heated, the physical aging-induced endothermic peaks disappear. This is the reason endothermic peaks were not observed in the 2nd, 3rd and 4th DSC

heating runs. Therefore, the disappearance of the endothermic peaks after the first heating run, and the observation of endothermic peak temperatures lower than T_g were considered as evidence for physical aging.

Table 1. Summary of thermal analysis (DSC) results

Sample	Glass transition temperature ($^{\circ}\text{C}$)	Endothermic relaxation peak ($^{\circ}\text{C}$)	Endothermic peak area (J/g)
EP3-pc	70.9 ± 0.6	54.7	1.41
EP2-pc	73.9 ± 0.3	53.9	0.34
EP-pc	71.5 ± 0.7	46.6	0.71

pc - post cured

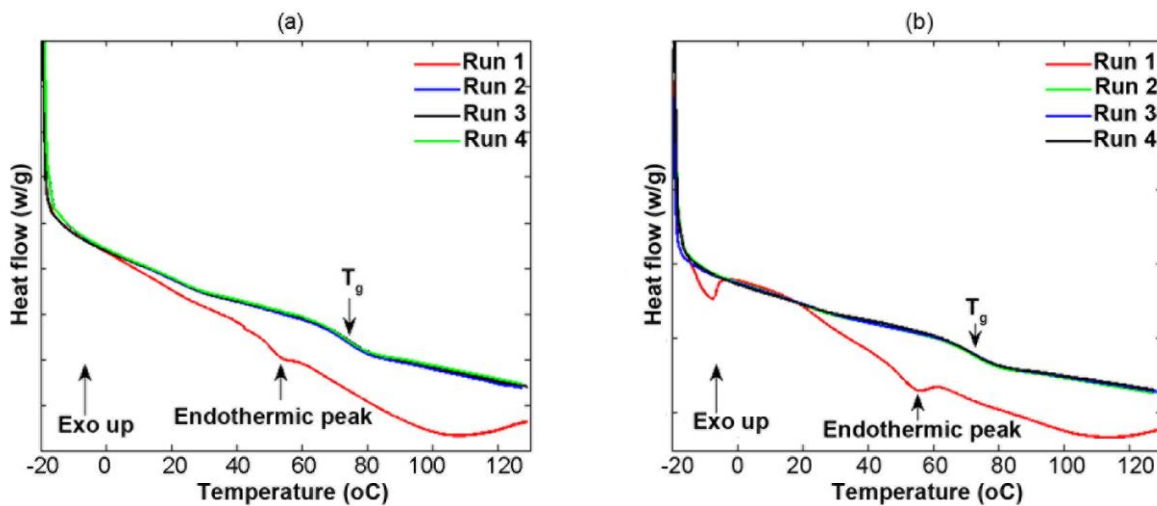


Fig. 4. DSC plots for post-cured (a) EP2 and (b) EP3 composite films

Further tests were conducted to establish whether the peaks in resistance observed during heating of as-cured samples (Fig.3) could be induced by first erasing the samples' thermal histories, followed by storage at temperatures lower than T_g so as to induce physical aging effects. Firstly, the thermal histories of as-cured samples were erased during monitoring of the change of resistance with temperature over two heat-cool cycles. Subsequently, the samples were stored (aged) at 23°C for 24h. Resistance measurements were once again

recorded during two heat-cool cycles after the 24h aging period. Fig. 5 shows the results for the heating runs from an EP2 sample, only. A resistivity peak near 60°C is clearly visible in plot A, first heating run (A - Run 1). A clear peak at this temperature cannot be seen for the second heating run (A - Run 2). After storage for 24h at 23°C, a small peak is again observed near 60°C during the first heating run (B - Run 1). The resistivity peaks near 60°C for the as-cured EP2 sample are more pronounced than those for the EP2 sample that was aged for 24h at 23°C after erasing the thermal history: note the increase in resistivity at ~60°C of about 6 times for plot A - Run 1 compared to a resistivity increase of about 1.5 times for plot B - run 1. For EP3 samples tested under the same conditions, the increase in resistivity at 60°C for a plot equivalent to A - run 1 was about 2 times, but a clear peak was not visible after 24h aging. The disappearance of the resistivity peaks was an indication that physical aging effects were erased during the first heating run, which was also shown by the DSC data in Fig. 4. The appearance of a small peak in resistivity around 60°C after aging in the case of EP2 sample, and not for the EP3 sample, indicates that the EP2 sample was in a higher non-equilibrium state compared to the EP3 sample. This may be due to the lower volume content of the MWCNTs in the EP2 sample, where the effect of physical change in the CNT network is likely to be more pronounced than in the EP3 sample due to fewer CNT interconnections and an overall less stable conducting CNT network.

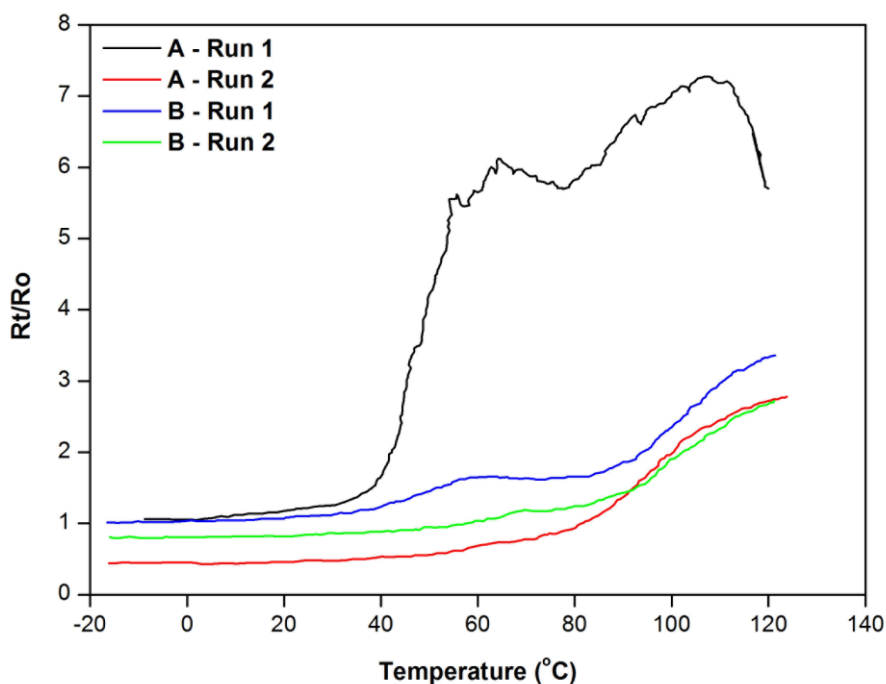


Fig. 5. Relative resistance versus temperature plots for an EP2 composite treated under different conditions (Plot A, Run 1: as-cured sample; Plot A, Run 2: as-cured sample after erasing its thermal history; Plot B, Run 1: sample used to generate data for plot A, runs 1 and 2 after storage (aging) at 23°C for 24 h; Plot B, Run 2: aged sample after erasing its thermal history)

The coincidence between the resistivity-temperature and heat flow-temperature responses, manifested in the appearance of both the endothermic relaxation and resistivity peaks near 60°C during the first heating run and disappearance in subsequent runs, was interpreted as evidence that the so-called PTC effect in conductive amorphous polymer composites is affected by the physical aging of the polymer phase. This agrees with what has been shown for carbon black-filled conductive amorphous polymer composites of the thermoplastics: polystyrene, poly(methyl methacrylate) and poly(vinyl chloride)²⁷, where storage time and temperature affected the magnitude of resistivity peaks observed near their respective glass transition temperatures. In the article cited above, a comment was made that these peaks were reminiscent of the enthalpic relaxation peaks observed via techniques such as DSC; however, there was no further explanation as to why these peaks in resistivity occurred. For cross-

linked amorphous polymer composites, such as those under study here, the effects of temperature cycling on the carbon nanotube network properties are likely to be different to thermoplastic systems as a result of decreased mobility within the cross-linked structure. In addition to the study here, a similar resistivity-temperature cycling phenomenon in epoxy/carbon black composites has been shown¹⁶, but the change in the profile of the temperature-resistivity plots as a function of cycle number was not discussed. Therefore, further study into the effects of this process on the carbon nanotube network is required and Raman spectroscopy may provide a method to do this.

Raman spectroscopy of the MWCNT/epoxy composites

To further study the observed physical aging effects on the MWCNT network in terms of strain transfer to MWCNTs, Raman spectroscopy was used. The Raman spectra of MWCNTs alone, an EP3 sample, an EP2 sample and an unfilled epoxy sample in the range 1200-3200 cm^{-1} at 25°C are shown in Fig. 6. For the MWCNT alone sample, significant bands that may be used to study the effect of strain on the nanotubes were observed. These were the D band at 1331 cm^{-1} , the G band at 1572 cm^{-1} and the G' band at 2652 cm^{-1} ³³, also known as the D* band in some literature³⁴. The Raman spectrum of the pristine epoxy shows prominent bands within the ranges 1200-1700 cm^{-1} and 2700-3200 cm^{-1} (Fig. 6d). Due to the absence of prominent bands in the 2660 cm^{-1} region in the Raman spectrum of the epoxy, the G' band of MWCNTs was selected to monitor the interaction of the polymer matrix and MWCNTs as a function of temperature. This band has been previously used to evaluate the effect of temperature on Raman band position in a MWCNT/epoxy composite at temperatures below T_g ³⁴. The Raman spectra of EP3 and EP2 in Fig. 6 (b) and (c), showed an expected relative decrease in epoxy Raman band intensity with increasing MWCNT content. The prominent G' Raman band of the MWCNTs at 2660 cm^{-1} can be clearly observed in both composite films.

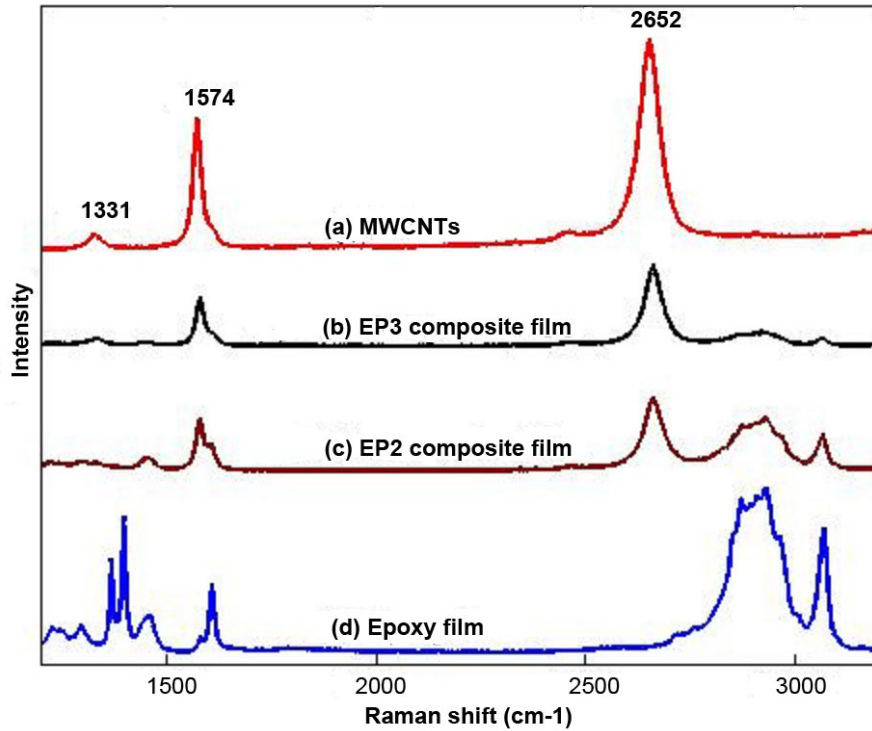


Fig. 6. Raman spectra in the range of 1200 - 3200 cm^{-1} at 25°C of (a) MWCNTs, (b) an EP3 composite film, (c) an EP2 composite film, and (d) an unfilled epoxy film

Table 2 presents a summary of G' Raman band positions for MWCNT powder alone and MWCNTs dispersed in epoxy. The results showed that embedding the MWCNTs in epoxy led to a shift in the G' band position toward higher wave numbers. This is consistent with what has been found for other CNT/polymer composites where hydrostatic compression of embedded CNTs causes an upward shift in the G' Raman band position³⁵. Fig. 7 shows the G' Raman band spectral region for the EP3 composite film at different temperatures. At elevated temperatures; above 90°C in the case of EP3 samples and 75°C in the case of EP2 samples, broad, featureless Raman spectra were obtained due to significant sample fluorescence. Therefore, the maximum temperatures used during this study were 90 and 75°C for EP3 and EP2, respectively.

Table 2. Raman band positions at 25°C for MWCNT powder and embedded MWCNTs in post-cured EP2 and EP3 composite films

Sample	G' band (cm⁻¹)
MWCNT	2652
EP3-pc	2661
EP2-pc	2661

pc = post cured

In the G' Raman band position-temperature plots shown in Fig. 8, there are peaks in the 55-60°C region. These peaks coincide with the range of enthalpic relaxation peak temperatures (Table 1) and the thermal history-dependent resistivity peaks near 60°C shown in the resistivity temperature plots (Fig. 3). A similar Raman spectral shift phenomenon has been observed for polyurethane acrylate (PUA) and bisphenol A polycarbonate (PC)/single-wall carbon nanotube (SWCNT) composites³⁶. Peaks in the Raman G' band position-temperature profiles of the SWCNTs were observed where polymer-phase secondary transitions and peaks from thermally-induced stresses were known to occur (from DMTA analysis); however, a specific mechanism behind these observations was not given. In our study, the agreement between the Raman band position-temperature data, the resistivity-temperature data, and the DSC data suggests that this phenomenon may be attributed to the disruption of the nanotube network as a result of epoxy matrix expansion and structural relaxation as the physical aging effects are erased during the heating process. All of these data help to achieve a greater understanding of the temperature-related phenomena observed for carbon nanotube/epoxy composites. A schematic of the proposed volume expansion-temperature process in the as-cured MWCNT/epoxy composites and its effect on the CNT network structure at the point of enthalpic/stress relaxation is shown in Fig. 9.

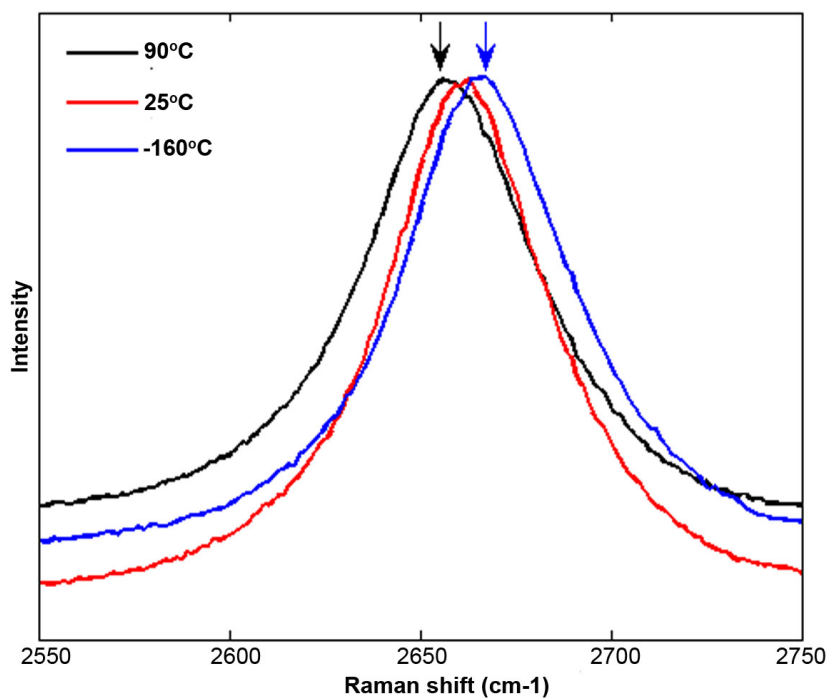


Fig. 7. Raman spectra from the EP3 composite film in the range 2550 - 2750 cm^{-1} showing the G' band shift from 2667cm^{-1} at -160°C to 2657cm^{-1} at 90°C

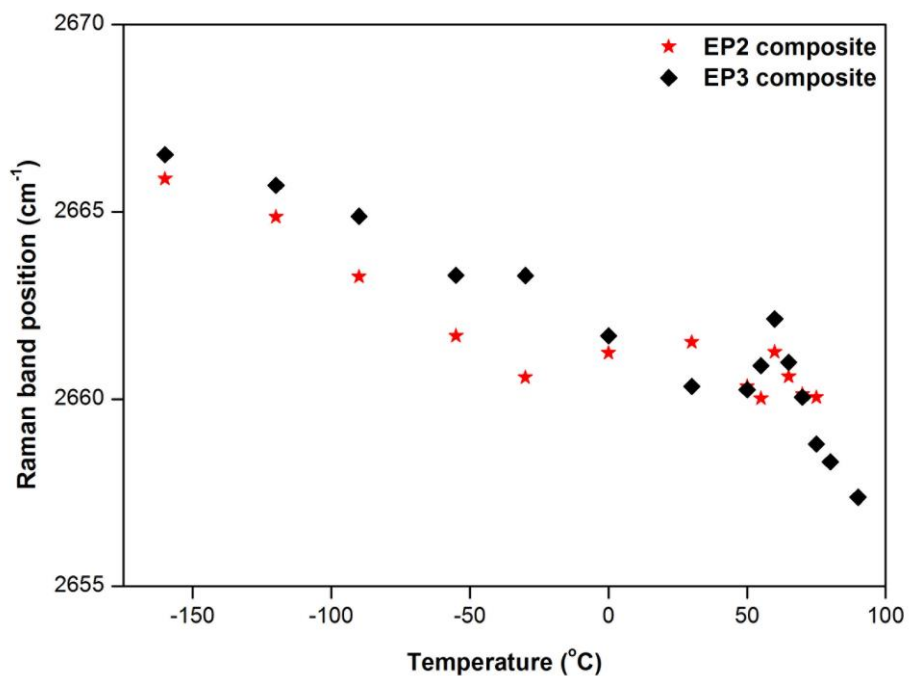


Fig. 8. Raman band position-temperature responses for the G' bands from EP2 and EP3 composite films

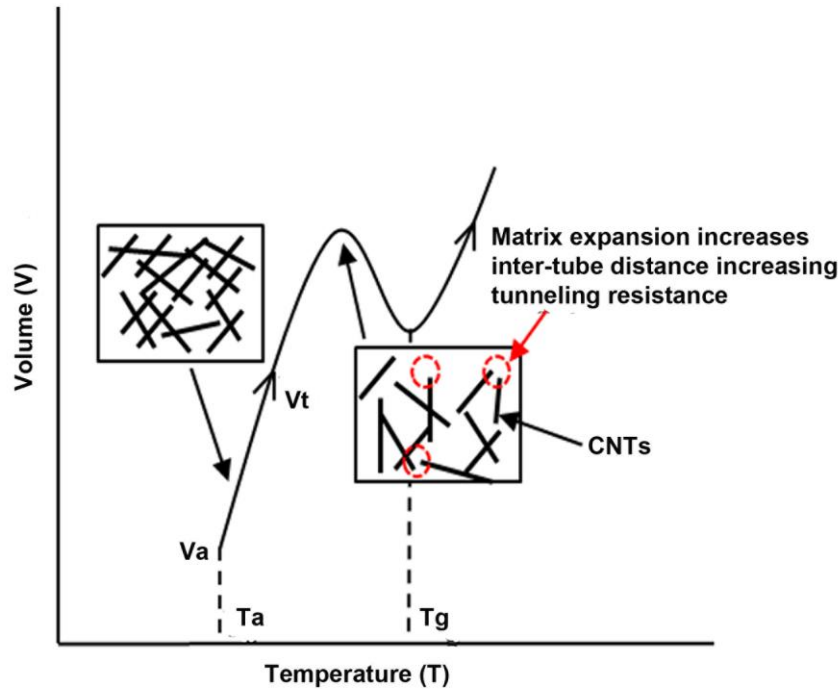


Fig. 9. A schematic illustration of predicted volume change and corresponding inter-CNT distance change as a function of temperature for as-cured MWCNT/epoxy composites. This schematic is based on data collected from resistivity-temperature, DSC and Raman spectroscopy measurements

4. CONCLUSIONS

Investigations into the temperature dependence of electrical resistivity in MWCNT/epoxy composite thin films revealed a high sensitivity to temperature change. Three regions were observed in the resistivity temperature plots for the composites: two main, consistent regions, below and above T_g and a thermal history-dependent region at temperatures close to the glass transition temperature. The thermal history-dependent regions corresponded to enthalpic relaxation peaks found during thermal analysis using DSC. In these regions, the electrical resistivity increased rapidly, resulting in peaks with six and two times the resistivity at room temperature for composites with 2 and 3% wt. MWCNT. This behaviour was found, however, to be dependent on the sample thermal history and only associated with the first heating cycle. Thermal and Raman spectroscopy analyses revealed that this behaviour can be

attributed to physical aging of the epoxy matrix phase and volume expansion induced structural rearrangement of the conductive network. Until now, a link between all of these phenomena had not been made for conductive carbon nanotube/epoxy composites and so these results add to the overall understanding of the PTC effect in such materials, with wider implications for the development of new devices for application in, for example, solar cells, supercapacitors, strain sensing, intelligent coatings etc.

Acknowledgements

The authors gratefully acknowledge the Australian Research Council (ARC) and the Queensland Government for providing financial support for this project.

References

1. N. Hu, Y. Karube, C. Yan, Z. Masuda and H. Fukunaga, *Acta Mater.* 56, 2929 (2008).
2. N. Hu, Y. Karube, M. Arai, T. Watanabe, C. Yan, Y. Li, Y. Liu and H. Fukunaga, *Carbon* 48, 680 (2010).
3. G. Yin, N. Hu, Y. Karube, Y. Liu, Y. Li and H. Fukunaga, *J. Compos. Mater.* 45, 1315 (2011).
4. N. Li, P. C. Eklund, Y. Huang, F. Du, X. He, X. Lin, H. Gao, Y. Ma, F. Li and Y. Chen, *Nano Lett.* 6, 1141 (2006).
5. T. Yamada, Y. Hayamizu, Y. Yamamoto, Y. Yomogida, A. Izadi-Najafabadi, D. N. Futaba and K. Hata, *Nat. Nanotechnol.* 6, 296 (2011).
6. H. G. W. Malte, T. B. Samuel, B. Lars, A. Rainer and S. Karl, *Nanotechnology* 19, 475503 (2008).
7. S. Huang, L. Li, Z. Yang, L. Zhang, H. Saiyin, T. Chen and H. Peng, *Advanced Materials* 23, 4707 (2011).

8. C. Peng, S. Zhang, D. Jewell and G. Z. Chen, *Progress in Natural Science* 18, 777 (2008).
9. E. Frackowiak, V. Khomenko, K. Jurewicz, K. Lota and F. Béguin, *J. Power Sources* 153, 413 (2006).
10. X. N. Guo, G. J. Zhi, Y. Y. Wang, G. Q. Jin and X. Y. Guo, *Carbon* 50, 321 (2012).
11. N. K. Shrivastava and B. B. Khatua, *Carbon* 49, 4571 (2011).
12. N. Hu, Z. Masuda, G. Yamamoto, H. Fukunaga, T. Hashida and J. Qiu, *Composites Part A* 39, 893 (2008).
13. Q. Wang, J. Dai, W. Li, Z. Wei and J. Jiang, *Compos. Sci. Technol.* 68, 1644 (2008).
14. R. H. Schmidt, I. A. Kinloch, A. N. Burgess and A. H. Windle, *Langmuir* 23, 5707 (2007).
15. N. Hu, Z. Masuda, C. Yan, G. Yamamoto, H. Fukunaga and T. Hashida, *Nanotechnology* 19, 215701 (2008).
16. J. Fournier, G. Boiteux, G. Seytre and G. Marichy, *J. Mater. Sci. Lett.* 16, 1677 (1997).
17. J.-i. Kim, P. H. Kang and Y. C. Nho, *J. Appl. Polym. Sci.* 92, 394 (2004).
18. J. Meyer, *Polym. Eng. Sci.* 14, 706 (1974).
19. L. Nicodemo, L. Nicolais, G. Romeo and E. Scafora, *Polym. Eng. Sci.* 18, 293 (1978).
20. H. Pang, Y.-C. Zhang, T. Chen, B.-Q. Zeng and Z.-M. Li, *Appl. Phys. Lett.* 96, (2010).
21. F. Kohler, *US Patents*, (1966).
22. K. Ohe and Y. Naito, *Jpn. J. Appl. Phys.* 10, 99 (1971).
23. H. M. Al - Allak, A. W. Brinkman and J. Woods, *J Mater Sci* 28, 117 (1993).
24. Y. P. Mamunya, H. Zois, L. Apekis and E. V. Lebedev, *Powder Technol.* 140, 49 (2004).

25. Y. Xi, H. Ishikawa, Y. Bin and M. Matsuo, *Carbon* 42, 1699 (2004).
26. C. Zhang, C.-A. Ma, P. Wang and M. Sumita, *Carbon* 43, 2544 (2005).
27. C. Klason and J. Kubát, *J. Appl. Polym. Sci.* 19, 831 (1975).
28. *Huntsman Corporation*, (2006).
29. D. Stauffer, *Introduction to Percolation Theory* (1985).
30. W. Bauhofer and J. Z. Kovacs, *Compos. Sci. Technol.* 69, 1486 (2009).
31. S. Carmona, E. Valot, L. Servant and M. Ricci, *Journal de Physique I* 2, 503 (1992).
32. L. C. E. Struik, *Physical aging in amorphous polymers and other materials*, Elsevier Amsterdam, (1978).
33. R. Saito, M. Hofmann, G. Dresselhaus, A. Jorio and M. Dresselhaus, *Advances in Physics* 60, 413 (2011).
34. O. Lourie and H. D. Wagner, *J. Mater. Res.* 13, 2418 (1998).
35. J. R. Wood, M. D. Frogley, E. R. Meurs, A. D. Prins, T. Peijs, D. J. Dunstan and H. D. Wagner, *J. Phys. Chem. B* 103, 10388 (1999).
36. Q. Zhao, J. R. Wood and H. D. Wagner, *J. Polym. Sci., Part B: Polym. Phys.* 39, 1492 (2001).